EXPERIMENTS ON PLASTIC BUCKLING OF STEEL BEAMS

By

M. IVÁNYI

Department of Steel Structures, Technical University, Budapest

Received January 20, 1973

Presented by Prof. Dr. O. HALÁSZ

1. Experimental analysis of plastic buckling

1.1 *Plastic instability*

In the mathematical treatment of stability problems involving the equilibrium condition of a structure, virtual disturbances are assumed, irrelevant to the force system [1]. Of course, however, in actual structures these disturbances are real ones, hence they affect not only the structure but the loading system. Therefore in stability tests, interaction of structure and loading system has to be pre-assessed.

Fig. 1 is an analysis of the effect of dead load (gravity load). Not all load types have characteristic curves like that in Fig. 1. In the so-called "spring load" systems, based on the principle of elastic reaction (e. g. screw-type testing machine, hydraulic jack) the load is transmitted from adjacent structures (straight line H—K in Fig. 2).

Accordingly, the equilibrium condition of a structure is stable if the gradient of the load-deflection curve of the structure g_s is more sloping than that of the load characteristic g_t. In general,

$$\text{the equilibrium condition is} \begin{cases} \text{stable} & g_s > g_t \\ \text{neutral} \quad \text{for} & g_s = g_t \\ \text{unstable} & g_s < g_t \end{cases}$$

The decisive majority of engineering steel structures are subject to gravity loads, hence covered by Fig. 1 so that the peak of the load-deflection diagram of these structures ($g_s = 0$) defines at the same time the point of neutral equilibrium, and so the failure load, of structures (maximum load).

But even under gravity loads, it may be decisive for a structure how the load-displacement diagram proceeds after peak C (Fig. 1), to be determined by tests, possible in turn only by applying the load type shown in Fig. 2 (so-called "spring" load).

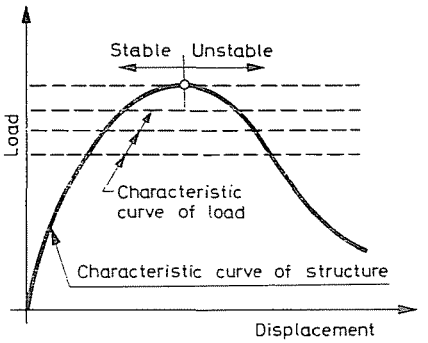

Fig. 1

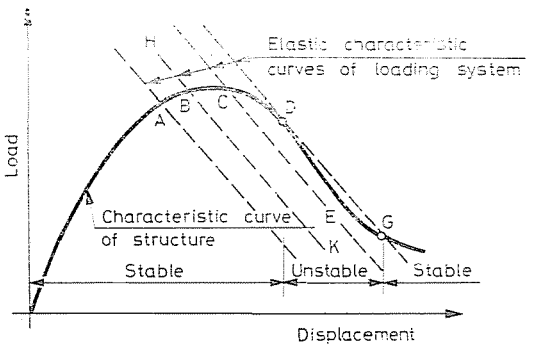

Fig. 2

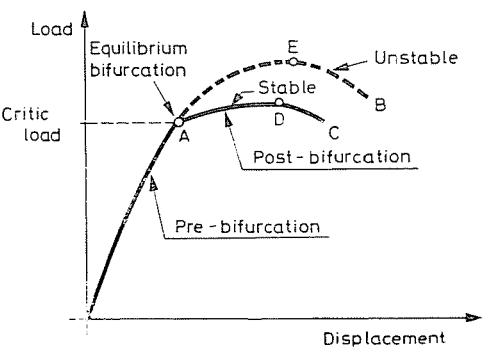

Fig. 3

1.2 *Bifurcation of the equilibrium*

The plastic instability described in the previous item is often preceded by bifurcation of the equilibrium, or buckling (Fig. 3).

The load-deformation relationship of a load-bearing structure loaded in increments may be assumed to be described by the curve OAB. In some

cases, however, at a given critical load, the deformed shape of the structure may suddenly change: the equilibrium bifurcates (point A in Fig. 3) [2].

Load-deformation diagram in Fig. 3 comprises two stable sections: OA previous to, and AC following the buckling as well as the unstable section AB. Buckling does not mean necessarily a structural failure; the curve section after buckling may be stable, hence failure may ensue from plastic instability.

In general, however, the buckling is considered the limit of serviceability of the structure.

Buckling may occur at any section of the original OAB curve, either in the elastic or in the plastic range.

Theoretical analyses and experiments on buckling problems in the plastic range have been recapitulated by M. J. SEWELL [3].

1.3 *Experimental investigation of the plastic buckling of steel beams*

For steel beams under uniform moment, if the maximum moment develops over a length rather than in a cross-section, a so-called "long" plastic hinge comes about.

Let us examine the load-displacement relationship for steel beams under uniform moment (Fig. 4).

The most comprehensive studies are likely to have been concerned with the buckling of beams in *range I*, hence, in the *elastic range* [4, 5].

Beams buckling in the *plastic range* i.e. *range II* [2, 5], have been examined for the influence of beam buckling on the moment bearing in the plastic range but its effect on displacements, deformations has been ignored.

Beams in *range III* also buckle in the plastic range, only that — besides of the possibility of the plastic moment to develop — their load capacity is exhausted only after a certain butt end rotation. Failure is due to the exhaustion of the "*plastic rotation capacity*" *of the beam.*

For the ultimate analysis of structures, the "plastic rotation capacity" has to be known, since not only the plastic moment M_t has to develop in the "plastic hinge" cross-section but also this moment has to be supported by the "plastic hinge" up to an adequate rotation, since plastic rotations are needed for the development of "yield mechanism".

Range IV includes beams with great moment reserves compared to the ultimate theory of first order, namely moments greater than plastic M_t can develop.

1.3.1. *Selection of the loading method.* In experiments where moment M acting at the end cross-section is to be produced by a gravity load, the horizontal curve section represents a neutral equilibrium condition (Fig. 5a),

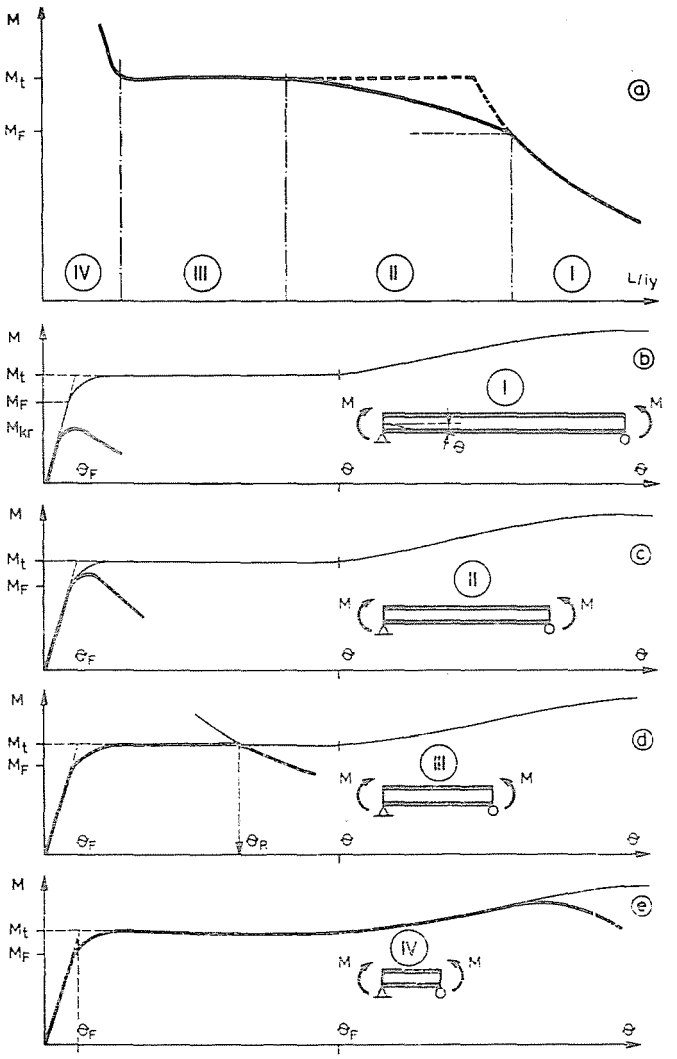

Fig. 4

where equilibrium bifurcation comes about at point A located in dependence of the beam span.

Naturally, point A is difficult to find by a gravity load test. If, however, the test is made in a screw-type testing machine, hence by means of a "spring" load, and the elastic characteristic curve of the testing equipment is arduous enough (Fig. 5b), the entire moment-rotation curve can safely be determined. $g_s > g_t$ being valid throughout; our tests can be made in stable equilibrium condition, hence the sloping branch of the $M - \Theta$ diagram, the load capacity decline can experimentally be observed.

Thus, "spring" load types can be stated to be convenient for testing the plastic buckling or the plastic rotation capacity of beams under uniform bending moments, of the so-called "long" plastic hinges, partly because of the peculiar behaviour of the beams — a section of the load-displacement diagram being horizontal, parallel to the displacement axis.

1.3.2. *Plastic buckling experiments described in publications.* Since in 1899 MICHELL, A. G. and PRANDTL, L. solved the problem of elastic buckling of rectangular beams, this problem has been treated in several papers and books, a quite detailed recapitulation being made by LEE, G. C. in 1960 [5].

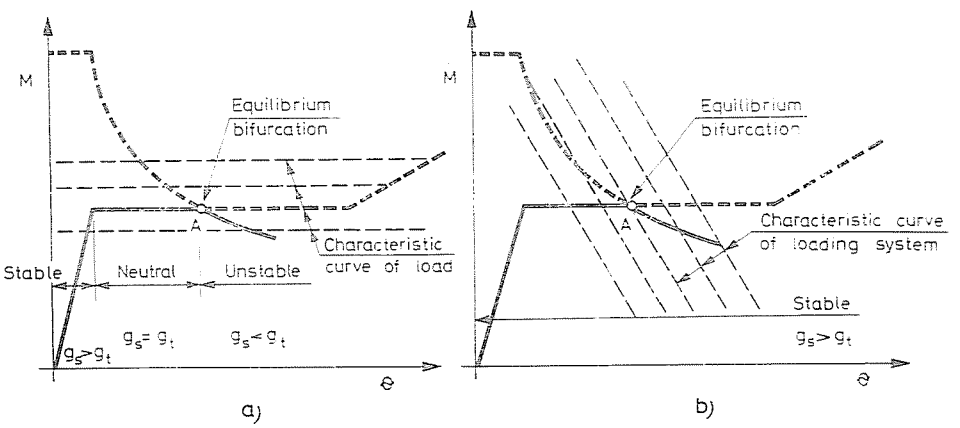

Fig. 5

In recent decades, two schools tested the plastic buckling of bending beams under uniform moments, i.e. those at the Universities of *Cambridge* (England) and of *Lehigh* (U.S.A.), respectively. The other test series made use of experience, results by one of both (MASSONNET, C. E., THÜRLIMANN, B., MASSEY, C., AUGUSTI, G. etc.).

1. *The Cambridge school* applied a multipurpose testing equipment for beam buckling tests, suitable also for column buckling, twist buckling, plate warping. The essential part of the testing equipment is the rig providing two supports, one being a fixed hinge, the other a roller hinge along the test beam axis [13].

The test series is featured by a supporting rig designed so that the end cross-section in line with the beam support can freely rotate in both principal directions of inertia but not at all normally to the beam longitudinal axis (from torsion aspect the end cross-section can be considered as restrained). Rotations in the horizontal plane being allowed by the supporting rigs (on ball bearings in the horizontal plane), the beams act as laterally hinged bars, simplifying the determination of the buckling length coefficient ($K = 1.0$).

Another feature of the test series is the gravity load applied on the loading cantilever outrigged from the supporting rig and much stiffer than the test beam (hence in the elastic range even beyond the load capacity of the test beam).

Test beams have been glued from steel plates.

AUGUSTI, G. and MASSEY, C. have been concerned with deformation problems of plastic buckling. AUGUSTI examined the plastic rotation capacity of the beam-columns. MASSEY [8] examined the plastic buckling of beams in bending under uniform moment. Deviation between actual and evaluated test data shows gravity load to be inconvenient, permitting no clear view of the end cross-section rotation where the beam load capacity began to decline (see Fig. 5a).

2. Since nearly two decades, the *Lehigh school* has been concerned with directives, specifications of the plastic design of steel structures [9], involving several tests on plastic buckling.

Test beams were rolled 8 WF 31 sections supported at third points, loads acted at the two ends, hence the middle third of the test beam was subject to a constant bending moment [2].

The load was transmitted by two hydraulic jacks ("spring" type load), hence, according to Fig. 5b, the moment end cross-section rotation or, generally, the load-displacement relationship could always exactly be traced.

All four lateral supports were plates perpendicular to the test beam. This way of supporting permitted the supported cross-section to rotate in both principal directions x and y of inertia, but inhibited rotations normally to the longitudinal axis of the beam. The rotation of the cross-section about the $x-y$ axis is, however, affected by adjacent beam spans, to be considered in determining the buckling length.

Lateral supporting plates were generally displaced (slipped) during the tests, prejudicial to the comparability of experimental and theoretical results.

LEE, G. C. and GALAMBOS, T. V. [6] were the first to experimentally investigate the plastic rotation capacity of the beam. Based on the former results, LAY, M. G. and GALAMBOS, T. V. [7] studied the relationship between the plastic rotation capacity and the length of the so-called "long" plastic hinge.

1.4 *Objective of our experiments. Testing program*

1968 to 1972, in the Laboratory of the Department of Steel Structures of the Technical University, Budapest, a test program has been established and performed on the plastic buckling of steel beams.

The experiments were to determine how close to place the lateral supports to promote the development of plastic moment M_i in steel beams under uniform moments. (Range III in Fig. 4). Hence, the beam buckling problem

was stated as to in what deformation state, for what value of end cross-section rotation Θ will the beam under plastic moment M_t fail by lateral rotation.

The plastic deformability of the beam is defined as its "plastic rotation capacity":

$$R = \frac{\Theta_R}{\Theta_F} - 1 \tag{1}$$

where Θ_R butt end rotation at plastic moment bearing;

Θ_F butt end rotation of a beam assumed to be elastic up to the development of plastic moment M_t.

Determination of rotation capacity of the so-called "long" plastic hinge is a special chapter of beam analysis for plastic buckling.

Assuming a uniform moment, rotations, curvatures and flange strains are related as:

$$\frac{\Theta}{\Theta_F} = \frac{\varkappa}{\varkappa_F} \cong \frac{\varepsilon_{\text{avg}}}{\varepsilon_F}. \tag{2}$$

Strains are measured at inner flange face [7]. This determination involves the assumption that ultimate moment M_t develops if flanges get into fully plastic deformation state. The behaviour of I-beams rather approaches this assumption.

The theoretical relationship of beam slenderness and plastic rotation capacity has been written in [12] making use of (1) and (2):

$$\frac{K \cdot L}{i_y} = \frac{\pi \sqrt{2E}}{D \sqrt{1 - \frac{R}{s-1}(h-1)}}. \tag{3}$$

Thus, *tests* were mainly intended as *starting* point for *theoretical analyses*, and aimed at *experimentally supporting theoretical results*.

Planning of the testing program had two important aspects to be reminded:

a) Lessons from published tests have been involved to plan a test series truly fitting theoretical considerations and directly supporting them. Therefore "spring" loading like that in Fig. 5b has been applied (Lehigh tests), and besides, adjacent beam parts have been designed so as to permit easy and exact observation of their effect on the tested beam section (Cambridge tests). Our test program did not involve the examination of the restraint due to adjacent beam parts.

b) New test methods were sought for, likely to offer a possibly wide-range insight into test beam behaviour, an overall view of the deformed con-

dition of the beam in plastic buckling. To this aim, the Department of Photogrammetry, Technical University, Budapest assisted our load tests by making normal stereophotographs.

The load scheme and the test program are recapitulated in Table I.

Table I

Test beam No.			L [mm]	Supports		
				A and D	B	C
G—1	G—11	G—21	147	Displacement and rotation in the vertical plane are permitted	Rotation in vertical plane permitted	Rotation in vertical plane and displacement along z axis permitted
G—2	G—12	G—22	196			
G—3	G—13	G—23	245			
G—4	G—14	G—24	294			
G—5	G—15	G—25	343			
G—6	G—16	G—26	392			
				Supports prevent displacements normally to the z axis		
Schopper 5Mp ("spring" load)	Screw jack			Loading equipment		
Strain gauge Ind. trans. W—10	Photogrammetry Inductive transmitter W—50			Measurement method		

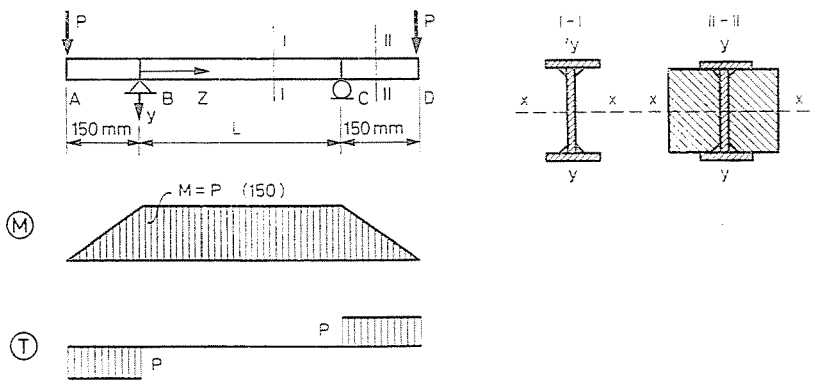

2. Tests: preparation and execution

2.1 *Test beam material*

In both theoretical analyses and tests, steel strain-hardening is taken into consideration, hence relevant material characteristics have to be determined. Test beams have been made of hot rolled plates and their material characteristics determined on tensile specimens of the form specified in Hun-

garian Standard MSz 105/59. Tensile tests have been made in a Schopper 5 Mp tensile tester ("spring" load), the tension has both been read off a mechanical dial, and continuously recorded on the Y axis by an $x-y$ plotter type EFK. The specimen extension change had to be recorded over a wide measuring range; to this aim an instrument had been constructed, consisting of two pickup jaws holding two inductive transmitters type W-10 bilaterally on the specimen (Fig. 6). Specimen extension had been recorded on the X axis of

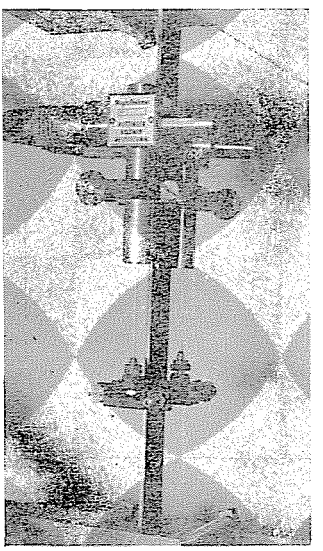

Fig. 6

the $x-y$ plotter as shown in Fig. 7 for 3 mm ∅ specimen C.14. $\sigma-\varepsilon$ diagram in Fig. 7a has been recorded, static yield point σ_{FS} being by definition that one essentially developing after a resting time of 15 min. 7b shows stress drop—time relationships for load intervals ①, ② and ③, demonstrating that no relaxation can be detected after about 15 min within the instrument sensitivity range.

The modulus of elasticity has been assumed as $E = 2100$ Mp/cm² (checked by measurements on two specimens). Neither the modulus of elasticity in shear G has been determined in tests but assumed as $G = 807.7$ Mp/cm².

The yield strain value ε_F has been determined without tests, but by definition as

$$\varepsilon_F = \frac{\sigma_{FS}}{E}. \tag{4}$$

Material characteristics for strain-hardening are relatively difficult to determine, the strain-hardening strain $\bar{\varepsilon}$ ought to be found by trial and error:

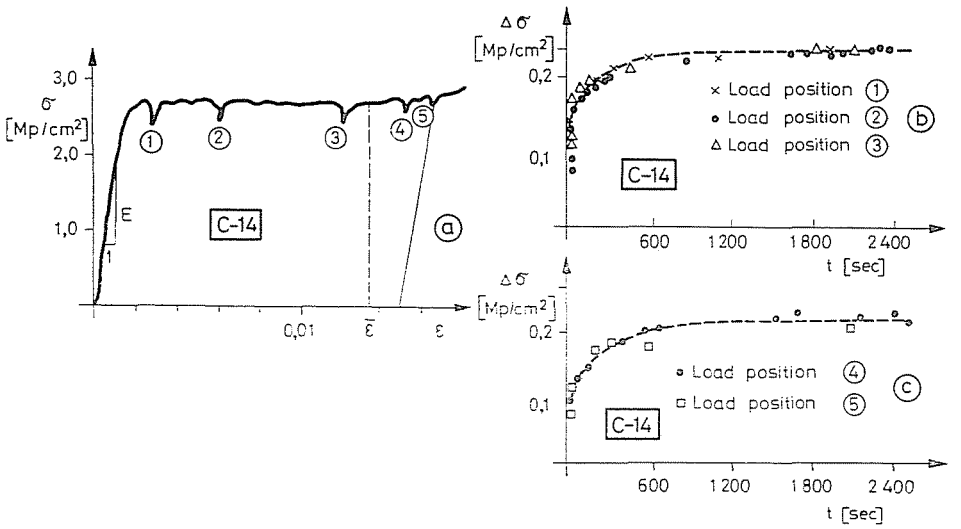

Fig. 7

Table II

Specimen symbol	Specimen number	σ_F	ε_F	E	$\bar{\varepsilon}$	$\bar{E}$	$h = \frac{E}{\bar{E}}$	$s = \frac{\bar{\varepsilon}}{\varepsilon_F}$
		kp/cm²	—	kp/cm²	—	kp/cm²	—	—
C (3 mm)	15	2410	0.00112	2100000	0.0136	6462	32.5	12.1
D (2 mm)	10	2380	0.001067	2100000	0.0126	6688	31.4	11.8

loading has often been stopped about the expected value, leaving a resting time of 15 min; the time where static stresses higher than the former value developed was accepted as the start of strain-hardening strain $\bar{\varepsilon}$. After this load interval ④, load interval ⑤ followed after a deformation value $\Delta\varepsilon = 0.0015$. The strain-hardening modulus value $\bar{E}$ has been determined in the interval of ④ and ⑤, the relevant relaxation—time relationship is seen in Fig. 7c to be similar to Fig. 7b.

Mean values of tests on tensile specimens are shown in Table II omitting details.

2.2 *Test beams and loading equipment*

Test beam flanges and webs were made of hot rolled steel plates 3 mm and 2 mm thick, respectively. At the place of flanges to take up web plates, grooves 1 mm deep and 2 mm wide have been milled to provide for the exact fitting of web and flanges (Fig. 8). Flanges and web have been joined by bilateral corner welding (under CO_2 shielding gas); to provide for a regular cross-

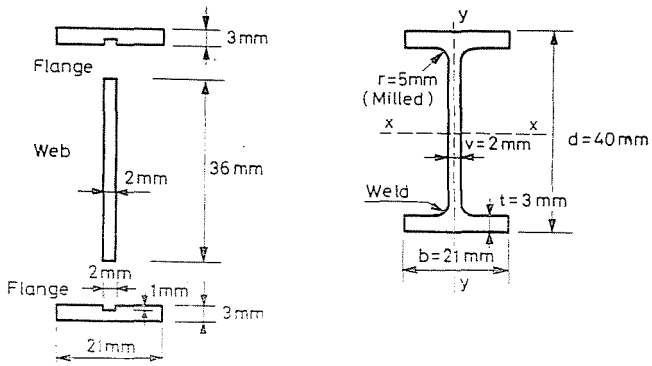

Fig. 8

Table III

Cross-section	Cross-section data				F	x—x axis				y—y axis	
	d	b	r	t		I_x	i_x	K_x	K_{plx}*	I_y	i_y
	mm				cm²	cm⁴	cm	cm³	cm³	cm⁴	cm
I 40	40	21	2	3	2.155	5.527	1.602	2.764	3.307	0.479	0.471

* [10]

$$K_{plx} = (F - vd)\frac{d-t}{2} + \frac{v \cdot d^2}{4} = 3.307 \text{ cm}^3$$

section, corner welds have been milled along by a 5 mm radius milling head. Because of the accurate machining, test beam sections had rather similar geometries, compiled in Table III.

The loading equipment is outlined in Fig. 9. Test beam length is $L+300$ mm (see in Table I), L being the test span. The 150 mm loading cantilevers were the same for every test beam: a thickened section has been applied to prevent yielding (section II—II in Fig. 9). Test beams were supported on fixed hinge B and on sliding hinge C through two ball bearings each, two vertical limbs of the loading rig being supported on ball bearings of the loading cantilever. Hinges B and C, as well as the vertical limbs of the loading rig could be adjusted for the test span.

2.3 *Test methods and tests*

Test series G-1 (Fig. 10)

The load has been determined both by the mechanic dial *dynamometer* of the loading equipment, and by a dynamometer of 5 Mp range.

Behaviour of the beam cross-section at mid-span has been determined by means of electrical strain gauges (Fig. 11). Displacement of the loading cantilever has been followed by an inductive transmitter W-10.

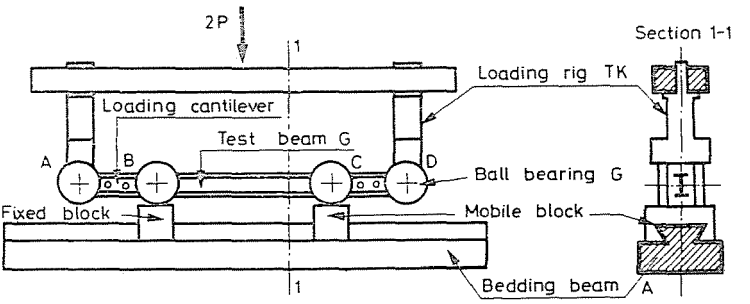

Fig. 9

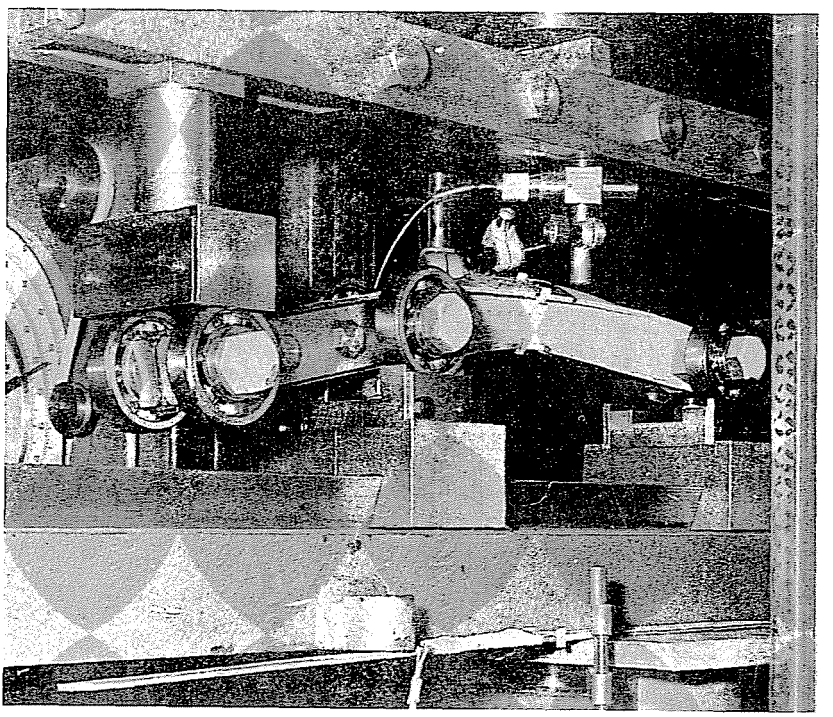

Fig. 10

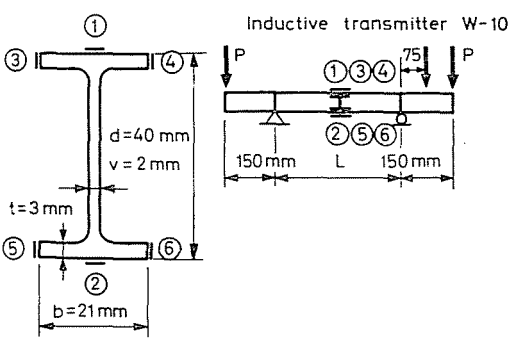

Fig. 11. ① ② SR—4 Type PFA—25—12; ③ ④ ⑤ ⑥ Huggenberger Type BP 2/120 p

Force change and deformation as well as displacement values have been recorded vs. time by means of a Honeywell 3508 Visicorder.

Test series G-11

Load has been applied via a screw-type testing machine, force being determined by a dynamometer of 5 Mp range, and recorded by an $x-y$ plotter type EFK. Displacement of the loading cantilever has been traced by an inductive transmitter W-50.

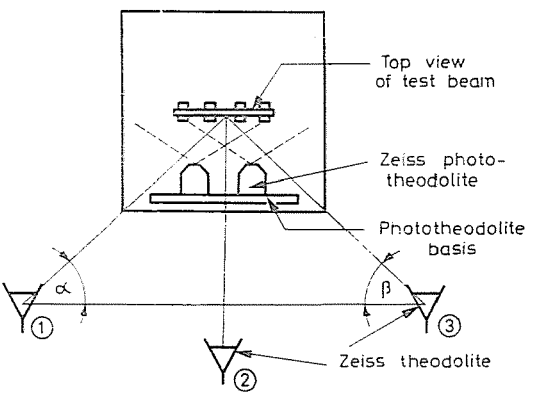

Fig. 12

Test beam displacements have also been determined by ground stereophotogrammetry [10, 11]. Stereophotographs (simultaneous, "two-eyed" shots) record the deformation state of the test beam at a given instant, for a determined load position. In course of the evaluation, in possession of inherent data of the measuring camera and of the two photo bases, the spatial position of any marked point could be determined.

Photogrammetric pictures have been made by means of a phototheodolite type Zeiss 19/1318, and interpreted in a Zeiss stereo-comparator and a Zeiss stecometer. To make interpretation of photographs inambiguous, beam surfaces had been painted white and marked with crosses.

Simultaneously with photographs, measurements have been made by ground geodesic methods (Fig. 12). Beam deformations have been tested by means of three Zeiss Theo-010 theodolites, ① and ③ determining horizontal angles describing horizontal displacements of individual cross-section points, ② determining elevation angle values describing vertical displacements.

Test series G-21

Methods were the same as for test series G-11 except that a finer mesh of points has been plotted on the web (spaced apart by 5 mm in level with the

web plate), and that the phototheodolite, rather than on stands, has been moved along the rule in Fig. 13, to eliminate eventual stand displacements during long waiting times.

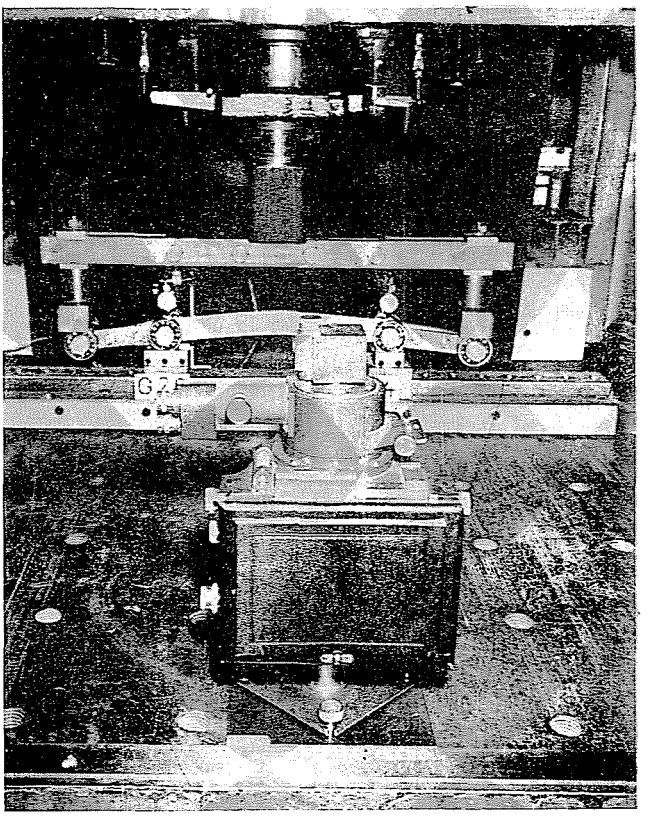

Fig. 13

Test procedure

After having adjusted the instruments, the load has been applied in load increments, with intervals of 15 min just as for the tensile specimens, namely here also, because of the "spring" type loading equipment, delayed deformations much affect load values, those sought for being static, rather than dynamic. After each 15 min waiting time, determinations have been made (reading off strain gauge values, taking photogrammetry pictures). In what follows, test data belonging to each load increment, recorded after waiting times, will be considered.

3. Evaluation of test results

Test results may be applied in different ways, such as:

— to facilitate development of the theoretical model, formulation of conditions, assumptions;

— to justify the correctness of the theoretical model, to demonstrate correlation between the model and the prototype.

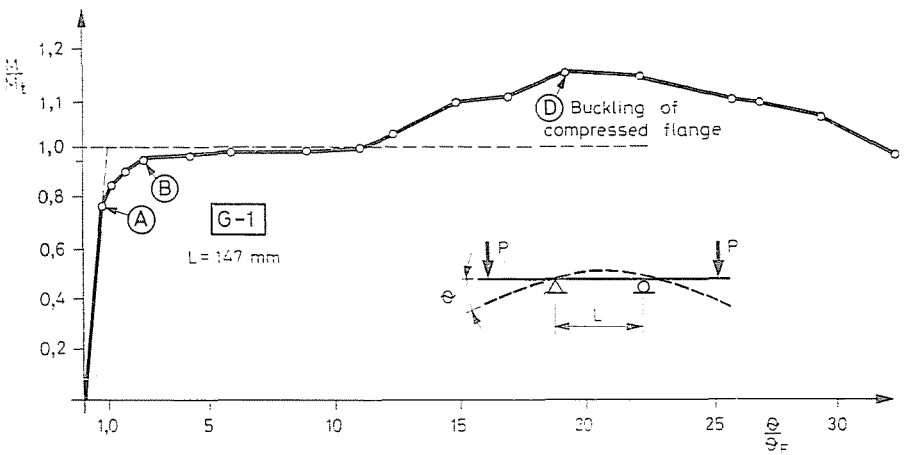

Fig. 14

Results of the three test series have been intended to fully represent the behaviour of the beam buckling in the plastic range, the so-called "long" plastic hinge. Tests tended fundamentally to two directions:

— to determine the load-displacement relationship, the load being applied by a bending moment in the vertical plane acting on end cross-sections B and C of the test span L (Fig. 9) as well as

curvature $\varkappa$

end cross-section rotation Θ due to the bending moment.

(For our analyses these relationships are of importance, hence they have been determined by several test methods.)

— to analyze the behaviour of parts (flanges, web) of the tested beam span.

3.1 *Results of test series G-1*

a) The moment — end cross-section rotation relationship $M—\Theta$ is seen in Figs 14 and 15 for beams G-1, and G-2 to G-6, respectively.

Vertical deflection of the loading cantilever had been determined by a Hottinger inductive transmitter type W-10; since the loading cantilever

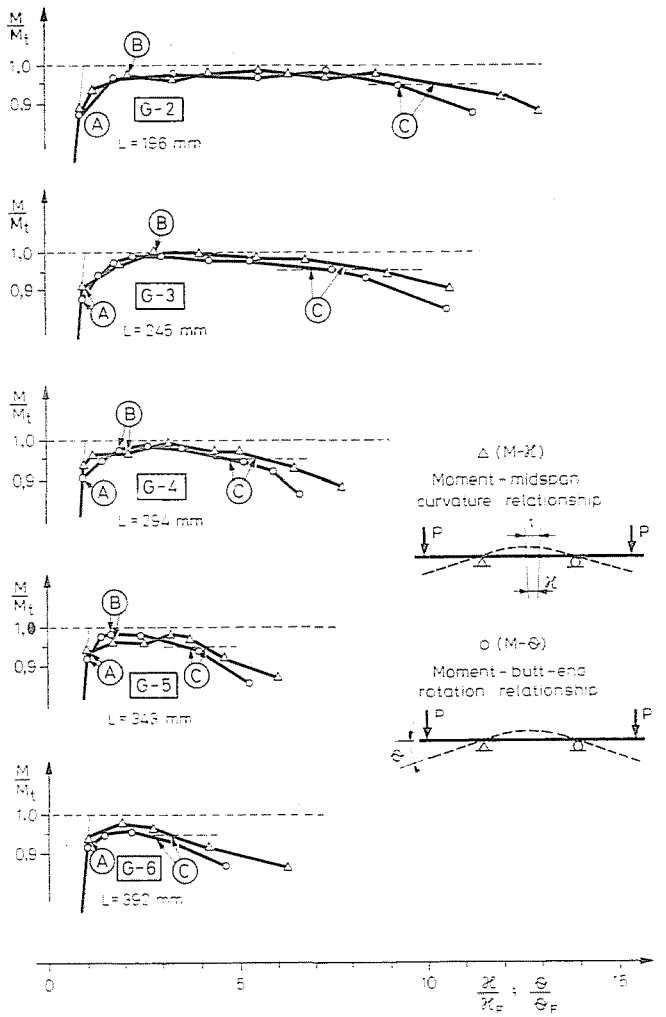

Fig. 15

had been reinforced (Fig. 9), its deflection value could be applied to determine the rotation in the vertical plane of the end cross-section of the tested beam.

It is obvious from the test results that the span of beam G-1 does not interfere with the development of the entire plastic rotation capacity, the strain-hardening even causes the $M-\Theta$ diagram after a nearly horizontal section to ascend, then to slope after a peak, indicating its load capacity to be exhausted. About the peak (point D in Fig. 14), buckling of the compressed flange appeared (Fig. 16).

Beyond the plastic moment M_f the beam G-1 is in range IV (Fig. 4). The $M-\Theta$ relationship is linear up to the first plastic deformation (point A

in Fig. 15), then, after about two or two and a half times of the end cross-section rotation Θ belonging to moment M_F, the plastic moment M_t is approached (point B in Fig. 15). The diagram shape between points A and B is influenced by the beam cross-section form and residual stresses. At plastic moment M_t, the $M-\Theta$ diagram becomes "horizontal".

At a difference from G-1, the $M-\Theta$ relationship of beams G-2 through G-6 becomes sloping after a "horizontal" section, indicating the exhaustion

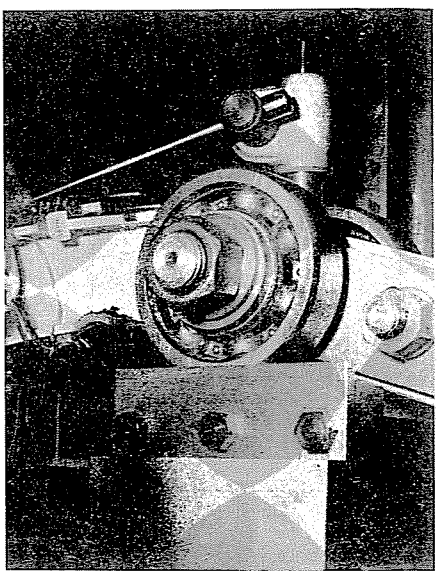

Fig. 16

of load capacity (point C in Fig. 15). The "horizontal" length depends on the beam span and it is characteristic of the plastic rotation capacity of the beam.

Beams G-2 through G-6 fail by excessive lateral displacement (Fig. 17).

b) $M-\varkappa$ i.e. moment – curvature relationship is shown in Fig. 15 for beams G-2 through G-6, as determined by two highly sensitive strain gauge foils SR-4 stuck at mid-span (Fig. 11).

Beyond the moment M_F for the first plastic deformation (point A in Fig. 15) the $M-\varkappa$ relationship is not linear any more, at two or two and a half times the curvature $\varkappa$ pertaining to M_F, the plastic moment M_t is approached (point B in Fig. 15), then also the $M-\varkappa$ diagram will be "horizontal", and after a "horizontal" length depending on the beam span it becomes sloping, and load capacity is declining [7] (point C in Fig. 15) at an assumed moment $M = 0.95M_t$ limiting at the same time the plastic rotation capacity.

According to Eq. (2), diagrams $M-\varkappa$ and $M-\Theta$ (Fig. 15) for each beam span ought to be similar quite up to failure (point C). The curves differ hardly up to, but markedly after M_i. Namely, the rotation in the vertical plane Θ has been determined from the vertical displacement of the loading cantilever, while the curvature $\varkappa$ from the cross-section deformation at mid-span. In course of test series G-1, small lateral displacements were observed

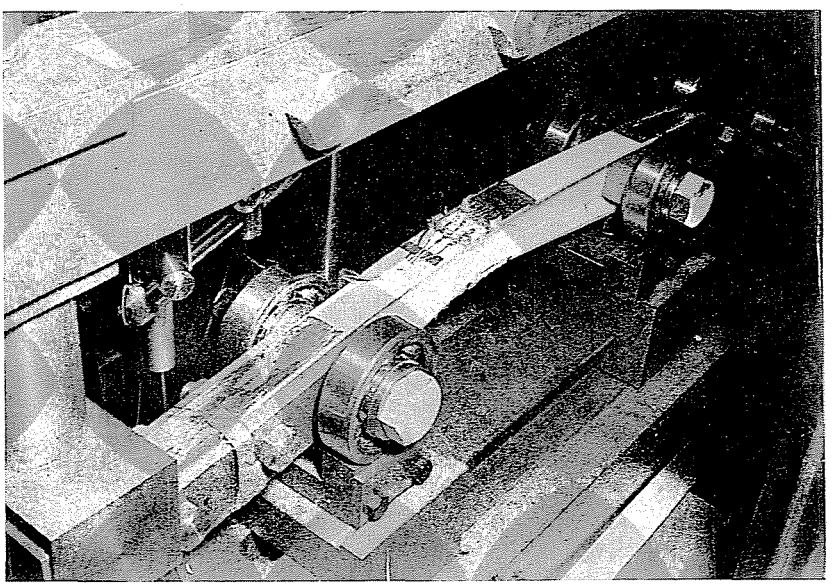

Fig. 17

near the plastic moment M_i so that both strain gauges indicated the combined effect of vertical and lateral displacements while the inductive transmitter W-10 is confined to the vertical displacement of the loading cantilever.

The deviation between both diagrams is, however, not as great up to failure (point C in Fig. 15) as to invalidate relationship (2). (Near point C the deviation averages 10 to 12 per cent.) Curves $\varkappa$ and Θ begin to significantly deviate after point C, indicating abrupt growth of lateral displacements.

Methods applied in test series G-1 permitted to examine actual, predetermined deformation characteristics, in course of the tests and evaluation, however, often in addition to the predefined deformational characteristics, the need of others arose for the analysis of beam buckling, hence, for the further test series, a method likely to give an insight into the deformation condition as a whole, has been sought for.

3.2 *Results of test series G-11 and G-21*

Test series G-11 has been decisively applied to determine the plastic rotation capacity, while test series G-21 was in addition intended to determine the moment and the lateral displacements (perpendicular to the moment plane).

a) Test series G-11

In addition to photogrammetry measurements, some characteristics have been determined by other methods such as the relationship of moment M to end cross-section rotation Θ. The $M-\Theta$ relationship has been continu-

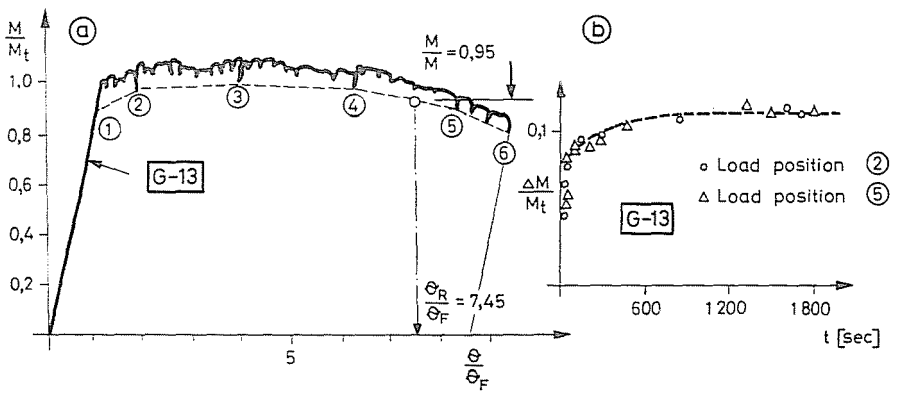

Fig. 18

ously recorded by a Honeywell x - y plotter. The $M-\Theta$ diagram for beams G-13 is shown in Fig. 18a.

The $M-\Theta$ relationship is affected by the loading system, just as is the $\sigma-\varepsilon$ relationship, hence after the load has been established, deformation decay had to be awaited.

The relationship between moment-"drop" ΔM and time t is shown in Fig. 18b. After 15 min of rest, the diagram is seen to have a nearly horizontal tangent, hence this waiting time is sufficient.

Photogrammetric pictures have been taken after the waiting time was off, measurement data are seen in Fig. 19. Inductive transmitter and photogrammetry data show a fair agreement.

b) Test series G-21

In addition to the analysis of the plastic rotation capacity, data from the relatively dense photogrammetric marks permitted to determine the relationship between the moment and the lateral displacements (perpendicular to the moment plane).

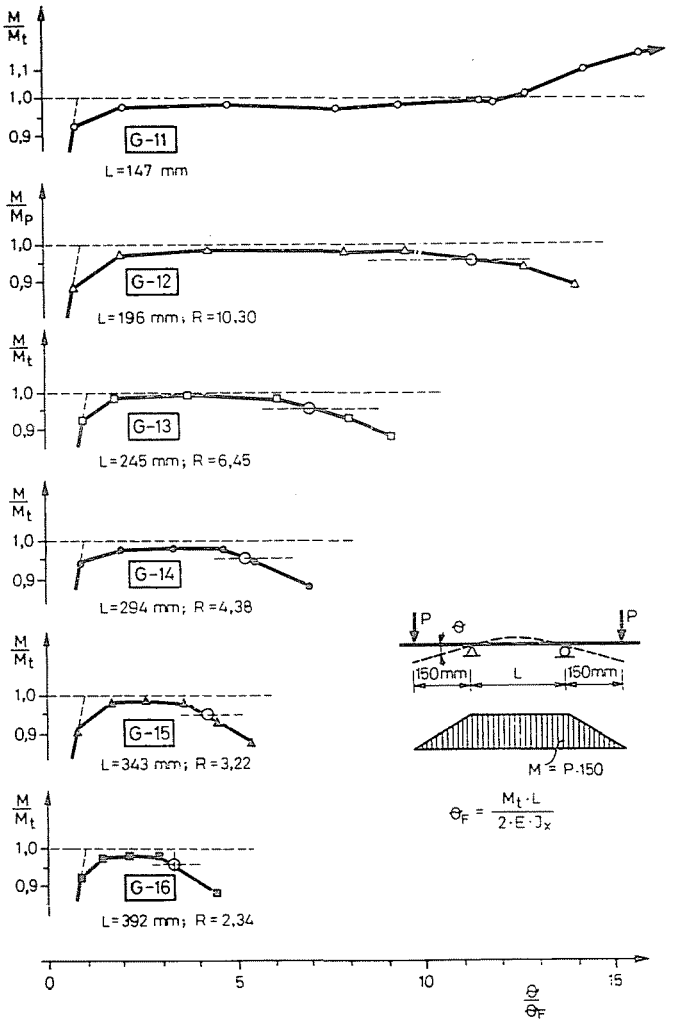

Fig. 19

Moment—end cross-section rotation $(M-\Theta)$ and moment—lateral displacement $(M-u)$ relationships for test beam G-22 are shown in Fig. 20. It is obvious from Fig. 20b that lateral displacements of the tensile flange are rather small, while those of the compressed flange are important. Somewhat below plastic moment M_t, the compressed flange exhibited slight lateral displacements, although according to theoretical considerations, no displacements in direction u were possible in this range; their occurrence may be attributed to manufacturing inaccuracies, load asymmetry. Up to the limit of plastic rotation capacity R, these displacements continue to grow even if

little, but after Θ_R the growth of lateral displacements quickens, so that they are visibly greater than those in the vertical plane.

c) Photogrammetric determinations permitted to analyze the deformed shape of each cross-section for different load positions. Fig. 21b contains displacements of cross-section ⑨ of test beam G-22 for load positions ③, ④

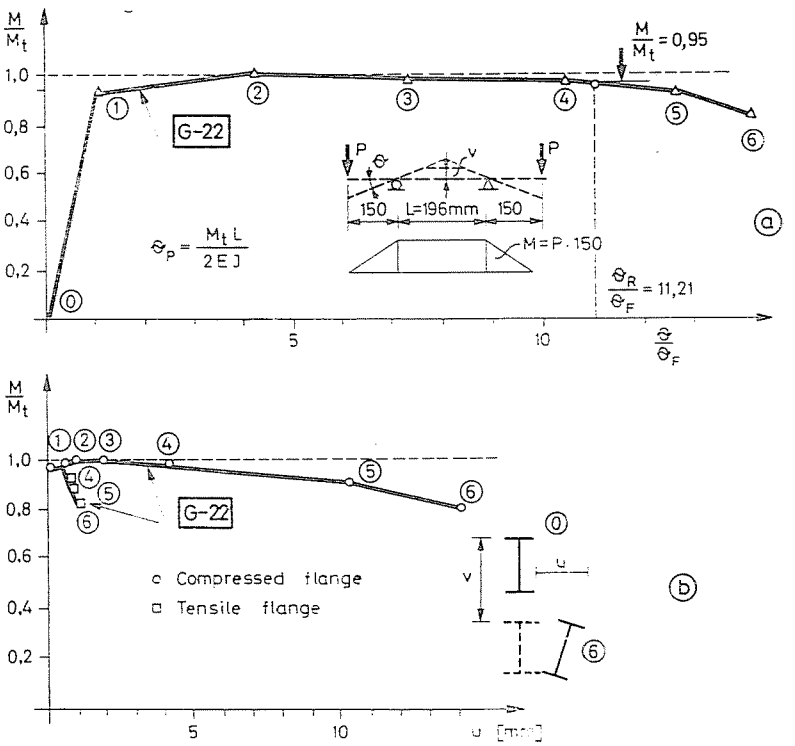

Fig. 20

and ⑤. Test results show the originally plain cross-section to remain nearly plain even beyond the plastic rotation capacity (load position ⑤ in Fig. 21).

Photogrammetric determinations have been checked by geodesic measurements (Fig. 12); displacements of a selected beam cross-section have been analyzed [11].

d) Photogrammetric determinations permit to determine lateral flange displacements for each load increment.

Lateral displacements of compressed and tensile flanges of test beam G-22 for load positions ③, ④ and ⑤ are shown in Fig. 22. Lateral displacements of flanges seem to verify the theoretical assumption that loading cantilever laterally brace the test beams resulting in a buckling length coefficient $K = 0.5$.

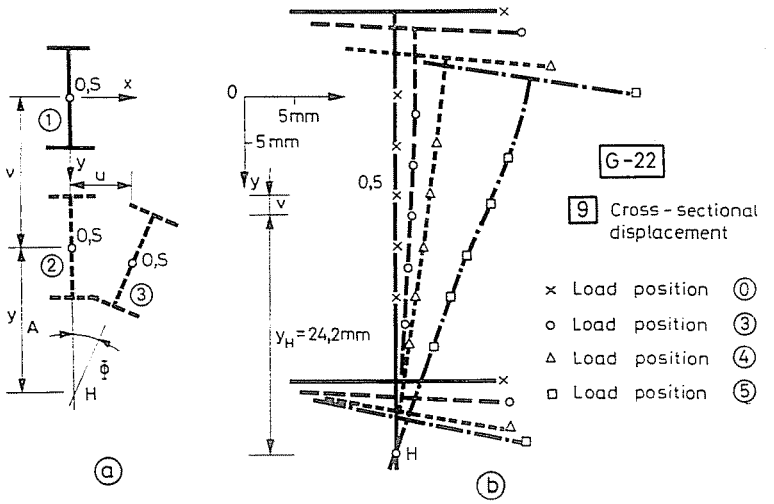

Fig. 21

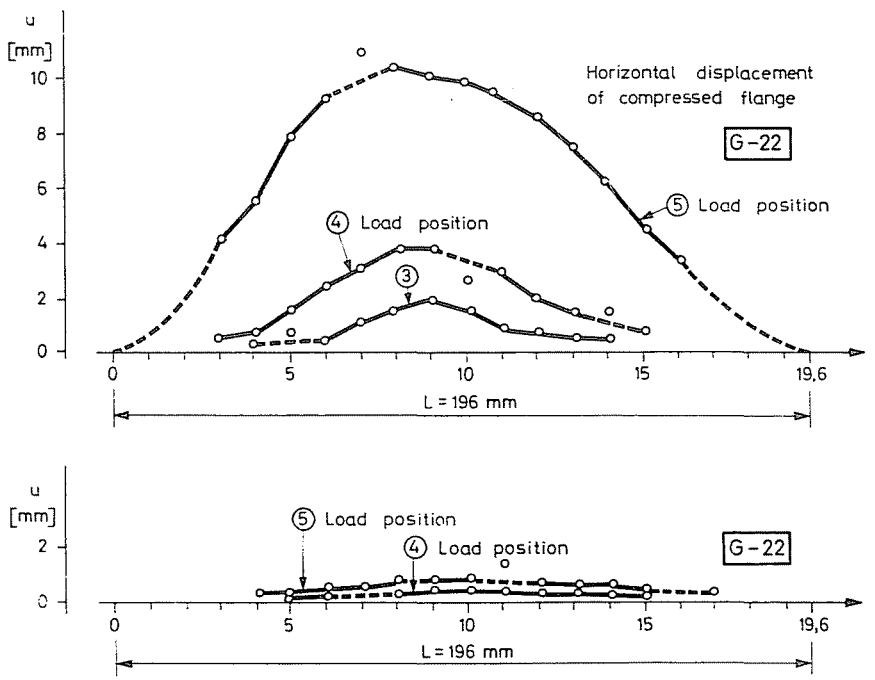

Fig. 22

Measurement results give a hint that in spite of the loading cantilever stiffness sufficient to laterally restrain the beam, supports B and C may allow slight horizontal rotations likely to reduce the assumed buckling length coefficient.

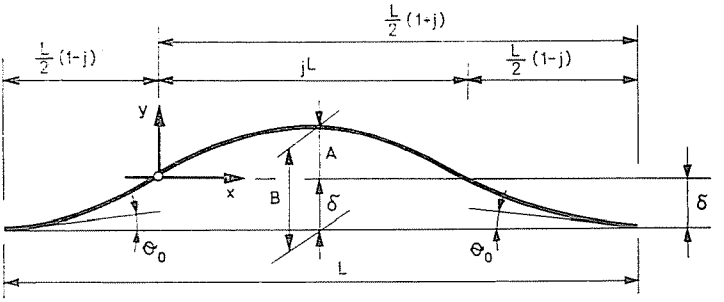

Fig. 23

Let us determine the buckling length coefficient for a slight horizontal rotation Θ_0 of the end cross-sections (Fig. 23).

Be the buckling form:

$$y = A \sin \frac{\pi x}{j \cdot L} . \tag{5}$$

Distance between the co-ordinate x axis and the end cross-sections:

$$\delta = - [y]_{x = \frac{L}{2}(1+j)} = - A \sin \left(\frac{\pi}{2j} + \frac{\pi}{2} \right) = - A \cos \frac{\pi}{2j} . \tag{6}$$

The tangent equation:

$$\frac{\mathrm{d}\, y}{\mathrm{d}\, x} = \frac{A \pi}{j \cdot L} \cos \frac{\pi x}{j \cdot L} . \tag{7}$$

Hence, the horizontal rotation of end cross-section Θ_0:

$$\Theta_0 = - \left[\frac{\mathrm{d}\, y}{\mathrm{d}\, x} \right]_{x = \frac{L}{2}(1+j)} = - A \frac{\pi}{j \cdot L} \cos \left(\frac{\pi}{2j} + \frac{\pi}{2} \right) = \frac{A \pi}{jL} \sin \frac{\pi}{2j} . \tag{8}$$

Maximum lateral displacement of the test beam for each load position:

$$B = A + \delta = A \left(1 - \cos \frac{\pi}{2j} \right) . \tag{9}$$

Substituted into (8):

$$\Theta_0 = \frac{B}{1 - \cos \frac{\pi}{2j}} - \cdot \frac{\pi}{jL} \sin \frac{\pi}{2j} . \tag{10}$$

Upon loading test beams, horizontal rotation Θ_0 of the end cross-section, and the maximum lateral displacement B could be measured and the reduced

buckling length factor j determined by iteration. (Load positions were selected for each beam so as to produce about equal maximum lateral displacements B. The Θ_0 to B ratio was assumed not to change in beam buckling.)

Measurement results and computation outputs are compiled in Table IV, omitting details. In evaluating test results, the reduced buckling length coefficient has been assumed with an average $j = 0.55$.

e) Comparison between test results and theoretical analyses of plastic rotation capacity in test series G-11 and G-21 is shown in Table V. (Theoretical analyses are described in [12].)

Table IV

Test beam No.	l [mm]	B [mm]	Θ_0	j
1	2	3	4	5
G—11	147			
G—12	196	0.31	0.01320	0.551
G—13	245	0.34	0.01280	0.546
G—14	294	0.30	0.00754	0.557
G—15	343	0.27	0.00827	0.538
G—16	392	0.29	0.00686	0.545
G—21	147			
G—22	196	0.33	0.01410	0.552
G—23	245	0.30	0.01090	0.548
G—24	294	0.31	0.00943	0.547
G—25	343	0.26	0.00635	0.551
G—26	392	0.28	0.00703	0.542

Columns 2 and 3 contain results obtained with the theoretical assumption $K = 0.5$; columns 4 and 5, values computed with the experimental reduced buckling length coefficient $j = 0.55$. Columns 6, 7 and 8, 9 show test results G-11 and G-21, respectively.

Photogrammetry measurement results can be applied to trace the entire displacement condition of the beam buckling in the plastic range for each load increment (position) (Fig. 7 in [11]).

4. Experimental results of plastic rotation capacity

The previously described three test series G-1, G-11, and G-21 refer to the plastic buckling of flexural beams, to the examination of plastic rotation capacity. Test results lead to the following conclusions:

Table V

Beam No	L [mm]	Theoretical $K=0.5$		Experimental $j=0.55$		Test results Series G—11		Series G—21	
		$\lambda=\frac{K\cdot L}{i_y}$	$\left(\frac{R}{s-1}\right)$	$\lambda'=\frac{j\cdot L}{i_y}$	$\left(\frac{R}{s-1}\right)$	$R_{11}=\frac{\Theta}{\Theta_p}-1$	$\left(\frac{R_{11}}{s-1}\right)$	$R_{21}=\frac{\Theta}{\Theta_p}-1$	$\left(\frac{R_{21}}{s-1}\right)$
	1	2	3	4	5	6	7	8	9
1.	147	15.60							
2.	196	20.80	1.113	22.90	0.913	10.30	0.927	10.21	0.920
3.	245	26.00	0.702	28.65	0.573	6.45	0.581	6.34	0.570
4.	294	31.20	0.476	34.40	0.386	4.38	0.394	4.26	0.384
5.	343	36.40	0.342	40.10	0.274	3.22	0.290	3.01	0.271
6.	392	41.60	0.253	45.80	0.202	2.34	0.211	2.19	0.197

1. The relationship between the critical moment M_{kr} and slenderness $jL\,i_y$ of beams under uniform moment is shown in Fig. 24.

Analysis of Fig. 4 showed beams of given slenderness to undergo plastic buckling at plastic moment M_t. Test results show the test beams to bear moments near the plastic moment M_t.

Beams G-1, G-11 and G-21 supported more than plastic moment M_t, these beams were characterized by full strain-hardening strain (Fig. 18).

2. Relationship between slenderness $\lambda'=jL\,i_y$ and plastic rotation capacity R of beams bending under uniform moment is shown in Fig. 25, together with theoretical analyses. Test results show a fair agreement with theoretical values (Table V).

3. Relative values of end cross-section rotation Θ and curvature $\varkappa$ for each test beam have been plotted in Fig. 15, demonstrating that although

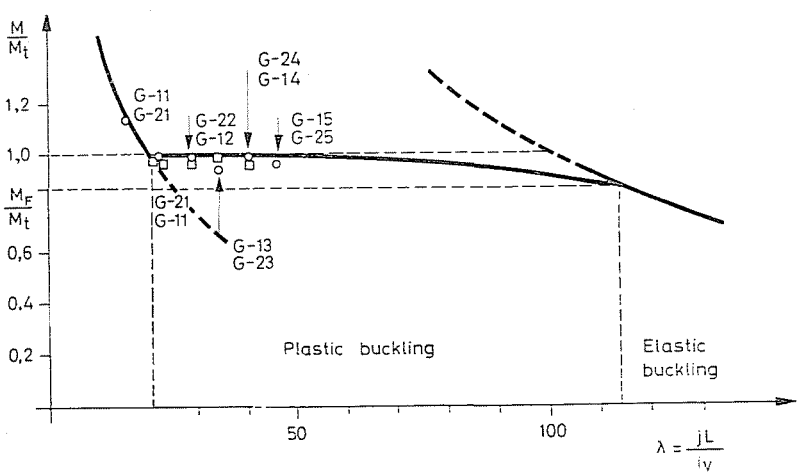

Fig. 24

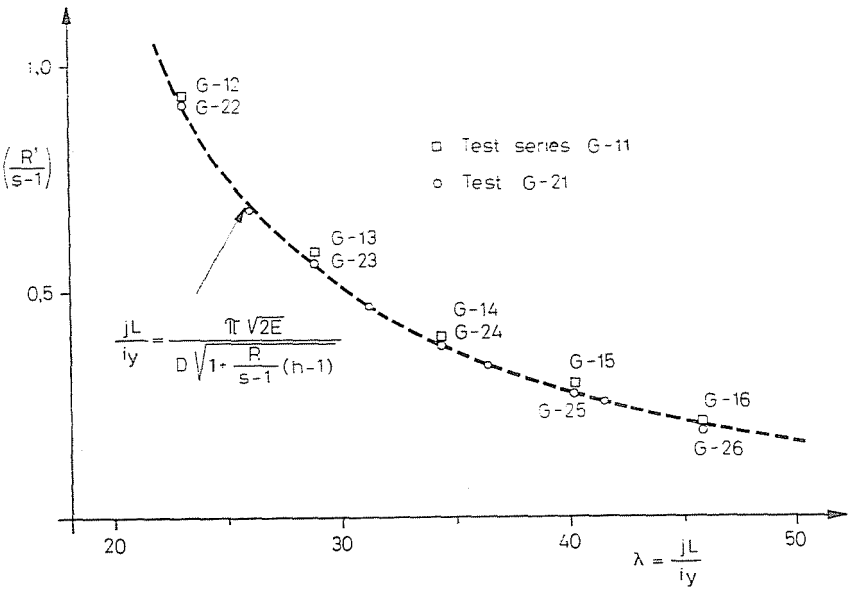

Fig. 25

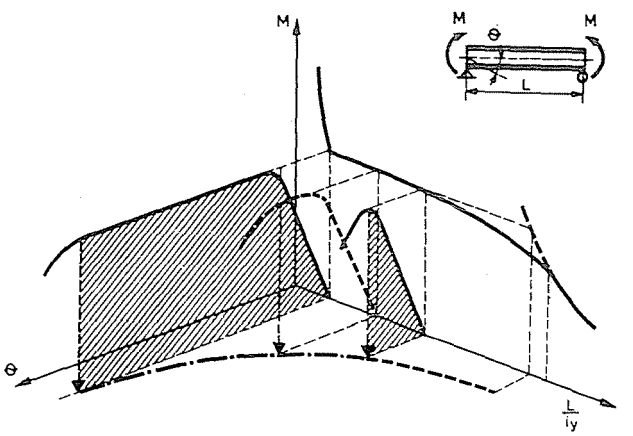

Fig. 26

measurement results of the two magnitudes Θ and $\varkappa$ are deviating near the exhaustion of load capacity, however, by less than to invalidate relationship (2).

4. Deformations of a cross-section of beam G-22 for given load positions have been plotted in Fig. 22. Even after exhaustion of the load capacity, the cross-section "rather" keeps its original profile, but laterally it is shifted and rotated.

5. Lateral flange displacements of beam G-22 are shown in Fig. 22 for various load positions; loading cantilevers laterally restrain the beam but

because of their design, supports allow a slight horizontal rotation reducing buckling length coefficient (Fig. 24; Table IV), however, to a moderate degree; an average reduced buckling length coefficient $j = 0.55$ has been applied.

Analysis of test results showed the photogrammetric measurement method to be a versatile means of checking theoretical assumptions, conditions, results, one of its great advantages being exactly to permit multiple uses, reclassification of its results, to offer a comprehensive insight, a deep-going analysis of the investigated phenomenon, making best use of the multitude of marks.

*

Essential features of the behaviour of flexural beams under uniform moment are shown in Fig. 26. The sides of load capacity $(M-L\,i_y)$ and of displacement capacity $(\Theta-L/i_y)$ are related by the moment-rotation relationship $(M-\Theta)$.

If no detailed analysis of the plastic rotation capacity of steel structures is desired, geometry data (span, cross-section) can be specified, likely to safely meet the requirement of displacement capacity, so that the "long" plastic hinge does not entrain "premature" loss of load capacity.

Codes in several countries permit plastic design of steel structures, Hungarian Standards MSz 15020/t and MSz 15 024/1 permit to determine stresses taking plastic deformations into consideration provided certain conditions are met. One condition is related to the spacing of lateral beam supports; our recapitulated experimental studies belong to this domain.

Notations:

A	buckling curvature amplitude
B	max. lateral beam displacement
b	flange width [cm]
d	depth of cross-section [cm]
E	modulus of elasticity [Mp/cm^2]
$\bar{E}$	strain-hardening modulus [Mp/cm^2]
F	cross-section area [cm^2]
f	shape factor $f = M_t/M_F = K_{pl}/K_x$
G	modulus of elasticity in shear [Mp/cm^2]
$h = E/\bar{E}$	
$J_{x,y}$	moment of inertia referred to gravity axes [cm^4]
$i_y = \sqrt{\frac{J_y}{F}}$	radius of inertia for the y axis [cm]
j	reduced buckling length coefficient
K	buckling length coefficient
K_x	modulus of cross-section [cm^3]
K_{pl}	plastic modulus of cross-section [cm^3]
L	beam span [cm]
$l = K \cdot L$	buckling length of beam [cm]
M	moment [cmMp]
M_t	plastic moment
M_F	moment at first yield

R	plastic rotation capacity
$s = \bar{\varepsilon}/\varepsilon_F$	
t	flange thickness
t	time [sec]
u, v	displacements in directions x and y [cm]
v	web thickness [cm]
x, y	co-ordinate axes of cross-section in the principal directions of inertia
z	longitudinal co-ordinate axis of the beam
$\Delta\varepsilon$	strain increment
$\Delta\sigma$	stress increment
ε	strain
ε_F	yield strain
$\bar{\varepsilon}$	strain-hardening strain
Θ	rotation of beam butt end (end cross-section)
Θ_F	butt end rotation of the beam assumed to be elastic up to ultimate moment M_f
Θ_R	butt end rotation at the exhaustion of moment capacity
Θ_0	rotation about the y axis of the beam end cross-section
$\varkappa$	curvature
$\varkappa_F$	curvature of the beam assumed to be elastic up to ultimate moment M_f
$\lambda = \frac{K \cdot L}{i_y}$	beam slenderness
$\lambda' = \frac{j \cdot L}{i_y}$	reduced beam slenderness
σ	stress [Mp/cm²]
σ_F	yield point [Mp/cm²]
σ_{Fs}	static yield point
σ_{Fd}	dynamic yield point
σ_0	limit of proportionality [Mp/cm²].

Summary

Buckling of beams in the plastic range under uniform moment, of the so-called "long" plastic hinges, has been experimentally investigated. Moment capacity and plastic rotation capacity of these beams has been determined. The experimental investigation has been applied as starting point for theoretical considerations, as well as for experimentally verifying theoretical results.

In addition to conventional test methods (strain gauges, inductive transmitters), the experiments involving three test series applied photogrammetry to obtain a deep insight into the beam behaviour: an overall view has been obtained of the deformation condition of beams buckling in the plastic range.

References

1. Hoff, N. J.: The Analysis of Structures. John Wiley and Sons, Inc. New York, 1956.
2. Galambos, T. V.: Structural Members and Frames. Prentice-Hall, Inc., Englewood Cliffs, N. Y. 1968.
3. Sewell, M. J.: A Survey of Plastic Buckling Stability. Ed. Leipholz, H.H.E. Solid Mechanics Division, Univ. of Waterloo, Canada, 1972.
4. Bleich, F.: Buckling Strength of Metal Structures. McGraw Hill Book Co., Inc., New York, 1952.
5. Lee, G. C.: A Survey of Literature on the Lateral Instability of Beams. Welding Research Council, Bulletin No. 63, August 1960.
6. Lee, G. C.—Galambos, T. V.: The Post-Buckling Strength of Wide-Flange Beams. Journ. of the Eng. Mech. Div. ASCE. Vol. 88., No. EM 1, 1962.
7. Lay, M. G.—Galambos, T. V.: The Inelastic Behavior of Closely Braced Steel Beams under Uniform Moment. Lehigh University Institute of Research, Fritz Eng. Lab. Report 297. 9, 1964.
8. Massey, C.: The Rotation Capacity of Steel I-Beams. British Welding Journal, Vol. 18., No. 8. August 1964.

9. Plastic Design of Multi-Story Frames. Lehigh University, Bethlehem, Pennsylvania, Fritz Eng. Lab. Report No. 273. 20. Vol. I—II. Summer Conference 1965.
10. HALÁSZ, O.—IVÁNYI, M.—KIS PAPP, L.: Photogrammetric Techniques in the Experimental Analysis of Instability Problems of I-Beams. RILEM International Symposium, Buenos Aires, 1971.
11. KIS PAPP, L.—IVÁNYI, M.: Issledovanie plasticheskoy pruchenosti stalnikh balok stereofotogrammetricheskim metodom. Per. Pol. C. E. Vol. 16. Budapest, 1972. No. 1—2.
12. IVÁNYI, M.: Buckling Analysis of Steel Beams in View of the Strain-Hardening Effect. (In Hungarian) C. Sc. Thesis, Budapest, 1972.
13. DAVIDSON, J. F.: The Elastic Stability of Bent I-Section Beams. Proc. Royal Soc. Ser. A. Math. and Phys. Sciences No. 1108. April 1952, Vol. 212.

Senior Assist. Dr. Miklós IVÁNYI, H-1521 Budapest